

Eradication of *Plasmodium falciparum* from Erythrocytes by Controlled Reactive Oxygen Species via Photodynamic Inactivation Coupled with Photofunctional Nanoparticles

Kang-Kyun Wang,^{†,||} Jin Woo Jang,^{‡,||} Eon Pil Shin,^{†,||} Hyung Wan Song,^{†,||} Jeong Wook Hwang,[†] Young Keun Kim,[§] Chae Seung Lim,^{*,‡} and Yong-Rok Kim^{*,†,||}

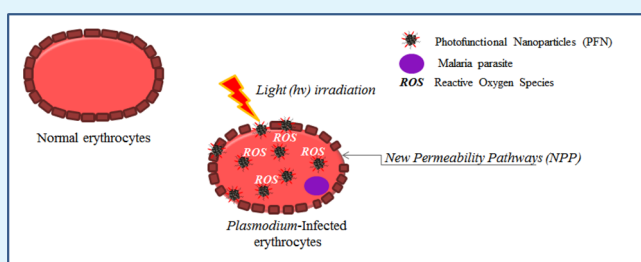
[†]Department of Chemistry, Yonsei University, Seoul 03722, Republic of Korea

[‡]Department of Laboratory Medicine, Korea University Guro Hospital, Seoul 08308, Republic of Korea

[§]Department of Materials Science and Engineering, Korea University, Seoul 02841, Republic of Korea

ABSTRACT: We investigated the antimalarial effect of photodynamic inactivation (PDI) coupled with magnetic nanoparticles (MNPs) as a potential strategy to combat the emergence of drug-resistant malaria and resurgence of malaria after treatment. Because the malarial parasite proliferates within erythrocytes, PDI agents need to be taken up by erythrocytes to eradicate the parasite. We used photofunctional MNPs as the PDI agent because nanosized particles were selectively taken up by Plasmodium-infected erythrocytes and remained within the intracellular space due to the enhanced permeability and retention effect. Also, the magnetism of Fe₃O₄ nanoparticles can easily be utilized for the collection of photofunctional nanoparticles (PFNs), and the uptaken PFNs infected the erythrocytes after photodynamic treatment with external magnetics. Photofunctionality was provided by a photosensitizer, namely, pheophorbide A, which generates reactive oxygen species (ROS) under irradiation. PAs were covalently bonded to the surface of the MNPs. The morphology and structural characteristics of the MNPs were investigated by scanning electron microscopy and X-ray diffraction (XRD), whereas the photophysical properties of the PFNs were studied with Fourier transform infrared, absorption, and emission spectroscopies. Generation of singlet oxygen, a major ROS, was directly confirmed with time-resolved phosphorescence spectroscopy. To evaluate the ability of PFNs to kill malarial parasites, the PDI effect of PFNs was evaluated within the infected erythrocytes. Furthermore, malarial parasites were completely eradicated from the erythrocytes after PDI treatment using PFNs on the basis of an 8 day erythrocyte culture test.

KEYWORDS: photofunctional nanoparticles, photodynamic inactivation, reactive oxygen species, Plasmodium, malaria, Plasmodium-infected erythrocytes



INTRODUCTION

Malaria is a mosquito-borne disease caused by Plasmodium species and is responsible for approximately 800 000 deaths a year worldwide.¹ The malaria epidemic is mediated by Plasmodium-infected mosquitoes; the parasite is transmitted to the human host after a blood meal; in the human host, the malarial protozoans parasitize erythrocytes and reproduce through self-replication.^{2,3}

Various antimalarial drugs have been developed for the treatment of malaria,⁴ such as antifolates, which suppress the synthesis of folic acid, which is essential for the proliferation of Plasmodium.^{1,5} However, these drugs have lost their efficacy due to the emergence of drug-resistant Plasmodium strains induced by overuse of quinolones and antifolates.^{6,7} Several research groups have recently reported the treatment of drug-resistance bacteria using the photodynamic therapy (PDT).^{8–10} In PDT, reactive oxygen species are generated through charge-transfer and/or energy-transfer processes from a photoexcited photosensitizer and induce apoptosis or necrosis of harmful

organisms by oxidation and/or activation of the signaling pathways.^{11–15} Baptista and colleagues showed that PDT could be used to treat various tropical diseases, including malaria.^{8,12} However, because general PDI agents can be taken up by noninfected erythrocytes, this method has limited practical application.¹⁶

In this study, we report enhanced photodynamic inactivation (PDI) of Plasmodium-infected erythrocytes by photofunctional nanoparticles (PFNs) and maintenance of the PDI effect of PFN over an extended period of time.

EXPERIMENTAL METHODS

Fabrication of PFNs. Magnetic nanoparticles (MNPs) were fabricated using the solvothermal reduction method reported previously.¹⁷ FeCl₃·6H₂O (98%), pheophorbide A (PA; 99%), 63

Received: December 30, 2016

Accepted: March 29, 2017

Published: March 29, 2017

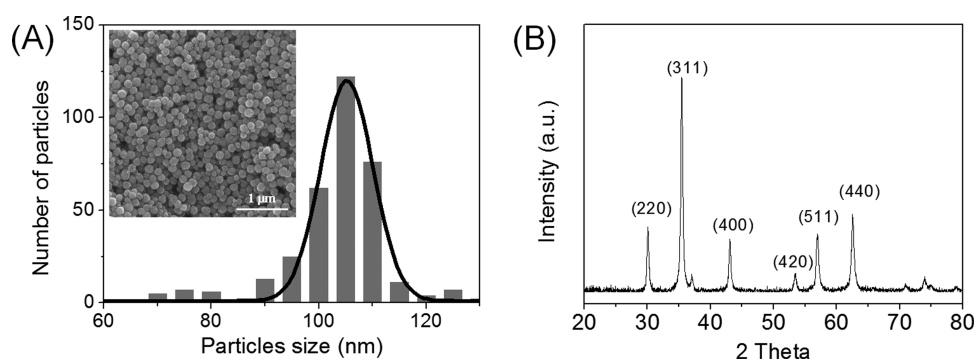


Figure 1. (A) Particle-size distribution of MNPs and SEM image (inset). (B) XRD pattern of MNPs.

64 polyethylene glycol (PEG; MW 1305–1595), ethylene glycol (EG; 65 99%), and NaAc (99%) were purchased from Sigma-Aldrich and used 66 without further purification. $\text{FeCl}_3 \cdot 6\text{H}_2\text{O}$ (1.35 g, 5 mmol) and PEG 67 (1.0 g) were completely dissolved in EG (40 mL), and then, NaAc 68 (4.69 g) was added to the mixture under vigorous stirring (200 rpm) 69 at 60 °C for 30 min. The viscous slurry was transferred into a Teflon 70 bottle in a solvothermal autoclave reactor.^{18,19} The autoclave was 71 heated and maintained at 200 °C for 12 h and then allowed to cool to 72 room temperature. Precipitates were collected after washing with 73 ethanol five times and were dried at 60 °C for 6 h. To fabricate PFNs 74 by the esterification reaction, MNPs (10 mg) were dispersed in the PA 75 solution (10 mL, 1.76×10^{-5} M in tetrahydrofuran (THF)). This 76 solution was agitated (200 rpm) at room temperature. After 24 h, the 77 product was washed with the THF solvent three times and then dried 78 at 60 °C for 6 h.¹⁷

79 **Instrumentation.** Field-emission scanning electron microscopy 80 (FE-SEM; JSM-6701F; Jeol Ltd.) was utilized to study the 81 morphology of the MNPs. The crystallographic structure of the 82 nanoparticles was investigated by X-ray diffractometry (XRD; Rigaku, 83 ultima IV) using Cu $K\alpha$ radiation. Fabrication of PFNs was confirmed 84 by Fourier transform infrared (FT-IR) spectroscopy using an FT-IR 85 spectrophotometer (Impact 400; Nicolet). Steady-state absorption and 86 emission spectra were obtained with a UV–vis spectrophotometer (U- 87 2900; Hitachi) and a spectrofluorimeter (F-4500; Hitachi), 88 respectively. The Nd-YAG (surelite II-10, 10 Hz, 7 ns; Continuum) 89 pumped optical parametric oscillator laser (OPO plus, 5 ns; 90 Continuum) was utilized as the excitation source ($\lambda_{\text{ex}} = 668$ nm) for 91 the detection of time-resolved singlet oxygen phosphorescence. The 92 phosphorescence signal was collected with a near-infrared photo- 93 multiplier tube (H10330A; Hamamatsu) at an angle perpendicular to 94 the excitation beam through cutoff (<1000 nm; CVI) and interference 95 filters (1270 nm; Spectrogon). The signal was amplified and acquired 96 by an amplifier (SR445A; Stanford Research Systems) and a 500 MHz 97 digital oscilloscope (DS07052A; Agilent Technology) and transferred 98 to a computer for further analysis.^{20,21}

99 **Biological Assays.** The light source for irradiation of PFNs was a 100 light-emitting diode (LED, $\lambda_{\text{max}} = 667$ nm, full width at half-maximum 101 (FWHM) = 79.6 nm, 6.58 mW/cm^2). LED light was radiated onto the 102 PFNs through a cutoff filter (<400 nm; CVI) to block the residual UV 103 light of the LED. The power density of the LED light at the sample 104 position was measured with a power meter (PM200; Thorlabs). To 105 evaluate the PDI efficiency of the PFNs, erythrocytes and *Plasmodium* 106 *falciparum* strain 3D7 (chloroquine-susceptible strain) were used. 107 Complete media consisted of Roswell Park Memorial Institute 108 (RPMI) 1640 supplemented with hypoxanthine, NaHCO_3 , human 109 plasma, gentamicin, and AlbuMAX I. To infect the erythrocytes, 110 erythrocytes (45.5×10^6 cell/mL) were cultured with *P. falciparum* 111 3D7 in complete media under a mixed gas phase ($\text{O}_2/\text{CO}_2/\text{N}_2 =$ 112 5:5:90) at 37 °C for 3 weeks.²² Infection of erythrocytes was evaluated 113 by Giemsa staining.²³ Of the erythrocytes, 10% were infected with *P.* 114 *falciparum* 3D7. The Plasmodium-infected erythrocytes were cultured 115 in the dark with various concentrations of PFNs (0–100 $\mu\text{g/mL}$) for 116 toxicity testing and were also cultured without PFNs under various 117 light-irradiation conditions (LED, $\lambda_{\text{max}} = 667$ nm, FWHM = 79.6 nm,

6.58 mW/cm^2 , 0–120 min) to test for light toxicity. The PFNs were 118 incubated with infected erythrocytes at room temperature for 24 h in 119 the dark to allow uptake. To evaluate the intracellular uptake efficiency 120 of PA and PFNs, PA (0.16 μM) and PFNs (25 $\mu\text{g/mL}$) were 121 incubated with Plasmodium-infected erythrocytes for 60 min at 37 °C. 122 The presence of PA and PFNs in the Plasmodium-infected 123 erythrocytes was assessed using a fluorescence microscope (iXon 124 EMCCD; Andor) and flow cytometric analysis (NAVIOS; Beckman 125 Coulter). In the case of flow cytometric analysis, RBCs were gated on 126 the basis of their forward scatter and side scatter signals with 127 logarithmic scales. At least 50 000 particles were assessed and plotted 128 in two-dimensional scattergrams of two of these three parameters, 129 FSC, SSC, and FL4 (Fluorescence Detector 4 (680–710 nm 130 emission)). PA and PFNs were detected in RBC areas with 131 fluorescence (FL2). The RBC area, PA area, and PFNs were detected 132 by analyzing the scattergrams from the computer software. 133

134 **PDI and Eradication of Plasmodium from Erythrocytes.** PDI 134 experiments were performed with various concentrations of PA and 135 PFN. The amount of PA molecules bonded to the surface of the 136 magnetic particles was estimated using UV–vis absorption spectroscopy. 137 Absorption optical densities (O.D.'s) at 667 nm were measured 138 with the initial PA/THF solution (1.85×10^{-5} M) before the addition 139 of magnetic particles for reaction and also with the PA/THF solution 140 that remained after reaction with the particles. The O.D. difference 141 between the initial and remaining PA/THF solutions indicated that 142 $\sim 6.49 \times 10^{-8}$ mol (equivalent to 3.9×10^{16} molecules) of PA was 143 immobilized onto the surface of 10 mg of magnetic particles. 144 Therefore, the number of PA molecules bonded to the surface of 145 the magnetic particles at 25, 50, 75, and 100 $\mu\text{g/mL}$ of PFN was 146 equivalent to the number of PA molecules in the liquid solution at 147 concentrations of 0.16, 0.32, 0.48, and 0.65 μM , respectively. In 148 experiments comparing PA and PFNs, the number of PA molecules 149 applied was kept the same. The applied concentrations were 0–0.65 150 μM PA and 0–100 $\mu\text{g/mL}$ PFNs. Plasmodium-infected erythrocytes 151 that were treated with PA or PFN were cultured for 24 h and then 152 placed in culture flasks under light irradiation with an LED ($\lambda_{\text{max}} = 667$ 153 nm, FWHM = 79.6 nm, 6.58 mW/cm^2) for 30 min. After 48 h, the 154 number of infected cells was estimated by Giemsa staining²³ and the 155 Plasmodium real-time polymerase chain reaction (RT-PCR) assay. 156 Eradication of the parasite was validated by evaluating Plasmodium 157 proliferation after 8 days of culture of the Plasmodium-infected 158 erythrocytes treated with PDI. The target genes of the RT-PCR were 159 circumsporozoite protein (CSP) and plasmodium lactate dehydrogenase 160 (pLDH) genes of *P. falciparum*. Plasmodium DNAs were extracted 161 from 100 μL of the PDI-treated samples using the QIAamp DNA Mini 162 Kit (Qiagen, Hilden, Germany). Briefly, each tube contained a 25 μL 163 reaction mix, which included 2.5 μL of isolated DNA, 0.1 μM of 164 forward and reverse primers, and 0.1 μM of the probe. TaqMan 165 amplification and detection were performed with a real-time 166 thermocycler CFX96 (Bio-Rad, Hercules, CA). Thermocycling 167 conditions were initial denaturation at 95 °C for 3 min, followed by 168 45 cycles at 95 °C for 15 s and 60 °C for 60 s. The RT-PCR analysis 169 indicates that the lower the threshold cycle (C_t) value, the more the 170 number of genes present. 171

RESULTS AND DISCUSSION

As shown in Figure 1A, the fabricated MNPs had good size uniformity. The size histogram of MNPs was obtained by

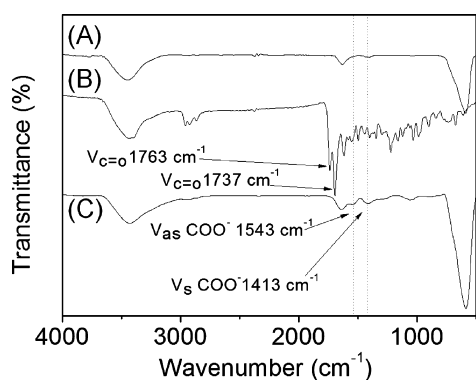


Figure 2. FT-IR spectra of (A) MNPs, (B) PA molecules, and (C) PFNs.

sampling 340 particles in different regions of the FE-SEM image. The average particle size was 103 ± 21 nm. The powder XRD pattern of MNPs provided detailed structural information, as shown in Figure 1B. The strong Bragg reflection peaks ($2\theta = 30.0, 35.6, 43.3, 53.7, 57.0, 62.8^\circ$) are marked by their Miller indices ((220), (311), (400), (422), (511), and (440), respectively), which were obtained from standard Fe_3O_4 powder diffraction data (card 19-0629; JCPDS). The position and relative intensity of all diffraction peaks corresponded to the characteristic peaks of a magnetite crystal with a cubic inverse spinel structure.^{17,19}

To understand the bonding nature of the carboxyl groups of PA and the Fe ions of MNPs, FT-IR spectra of all samples were compared, as shown in Figure 2. The IR spectrum of PA had absorption peaks at 1763 and 1737 cm^{-1} , which correspond to the stretching modes of the free carbonyl double bond ($\nu_{\text{C=O}}$) (Figure 2B).²⁴ After esterification between the carboxyl group of PA and Fe ion of MNPs, the peaks assigned to the free carboxyl group disappeared (1763 and 1737 cm^{-1}) and new bands appeared at 1543 and 1413 cm^{-1} , which we ascribed to the asymmetric (ν_{as}) and symmetric (ν_{s}) stretch vibrations of the carboxylate group (COO^-), respectively.²⁴ The appearance of these new bands was also reported in the IR study of Dravid and colleagues.²⁵ This pattern of spectral change is due to Fe-carboxylate complexation as a result of chemical coordination, as shown previously.²⁶

The photophysical properties of PFNs were characterized by steady-state absorption and emission spectroscopies. Figure 3A presents the characteristics of PA absorption bands: the Soret band at 410 nm and the Q bands at $504, 534, 608,$ and 666 nm were nearly identical for PA in THF solution and PFNs in THF solution.²⁷ The fluorescence emission peaks of PFNs in THF solution at 675 and 725 nm were also similar to those of PA in THF solution (Figure 3B). This suggests that the photophysical properties of PA are not altered by bonding between PA and MNPs.¹⁰

The most direct measurement method for singlet oxygen is the detection of phosphorescence from the deactivation of singlet oxygen molecules induced by photoexcited PA.²⁸ As shown in Figure 4, singlet oxygen phosphorescence signals from low concentrations of PA (0.016 μM) and PFNs (2.5 $\mu\text{g}/\text{mL}$) were measured in THF solution at a detection wavelength of 1270 nm to avoid light scattering from the MNPs. The intensities of the singlet oxygen phosphorescence signal at the zero time point were nearly identical for PA and PFNs in THF solution. The phosphorescence decay signals from PA and PFNs were fitted to a single exponential function, yielding similar singlet oxygen lifetimes of 22.7 and 22.1 μs , respectively. These measured singlet oxygen lifetimes are consistent with the reported value.²⁸ These results indicate that the same amount of singlet oxygen was generated from PA and PFN and that the singlet oxygen generated from PFNs did not undergo self-quenching by the interface modified MNPs.^{20,29}

To assess the toxicities of PFNs and irradiated light, Plasmodium-infected erythrocytes were cultured with PFNs in the dark or only with light irradiation in the absence of PFNs. PFNs were not toxic in the concentration range of 0 – 100 $\mu\text{g}/\text{mL}$, and no light toxicity in the energy range of 0 – 48 J was evident (see Figure 5).

The PA- and PFN-uptaken RBC counts are quantified as 11.7 and 23.8% , respectively. The more efficient uptake of PFNs compared to that of PA shown in Figure 6B is expected to be due to the enhanced permeability and retention (EPR) effect of the former.³⁰ The permeability of the erythrocytes increases during malarial infection due to the destruction of the spectrin network.³¹ Both PFNs and PAs can be taken up easily by Plasmodium-infected erythrocytes due to the induction of new permeability pathways by the malarial parasite.³² The uptaken PFNs accumulate in the Plasmodium-infected erythrocytes because of physicochemical pharmacological factors.^{16,32}

After 30 min of irradiation for PDI treatment, the infection rate of the erythrocytes decreased in a dose-dependent manner according to the concentrations of PAs and PFNs (Figure 7A).

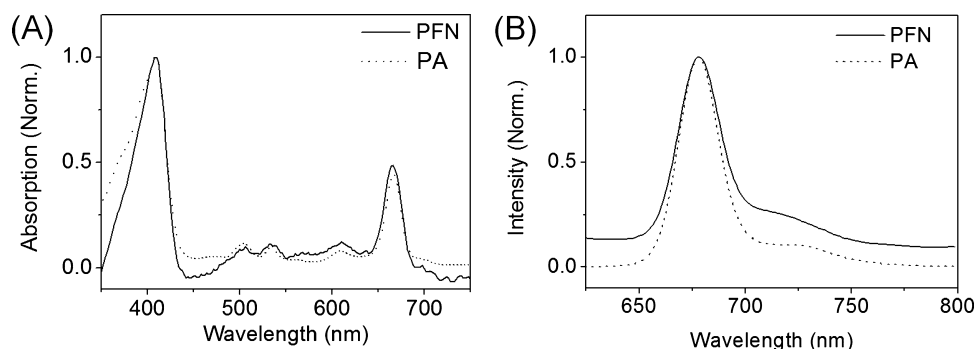


Figure 3. (A) Absorption and (B) emission spectra of pure PA and PFNs in THF. The excitation wavelength for the emission spectrum was 410 nm.

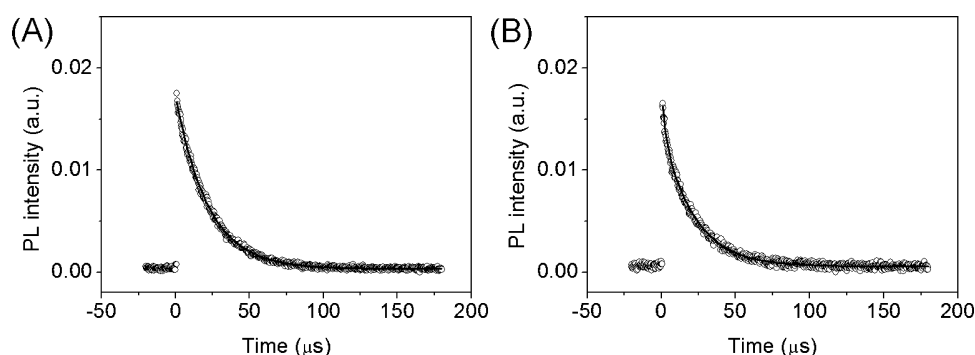


Figure 4. Phosphorescence decay signals induced by relaxation of the singlet oxygen from (A) PA and (B) PFNs in THF solution. Phosphorescence signals were detected at 1270 nm and fitted with a single exponential function (solid line).

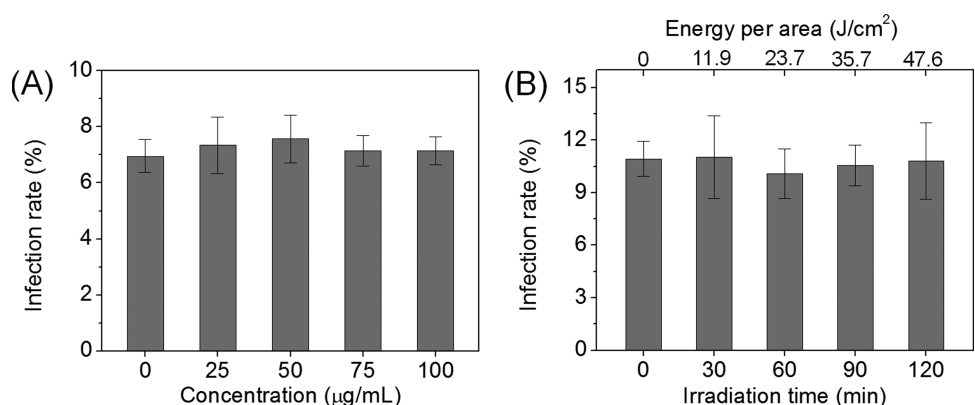


Figure 5. Toxicity test of (A) PFNs without light irradiation and (B) only under light irradiation without PFNs. These experiments were repeated three times.

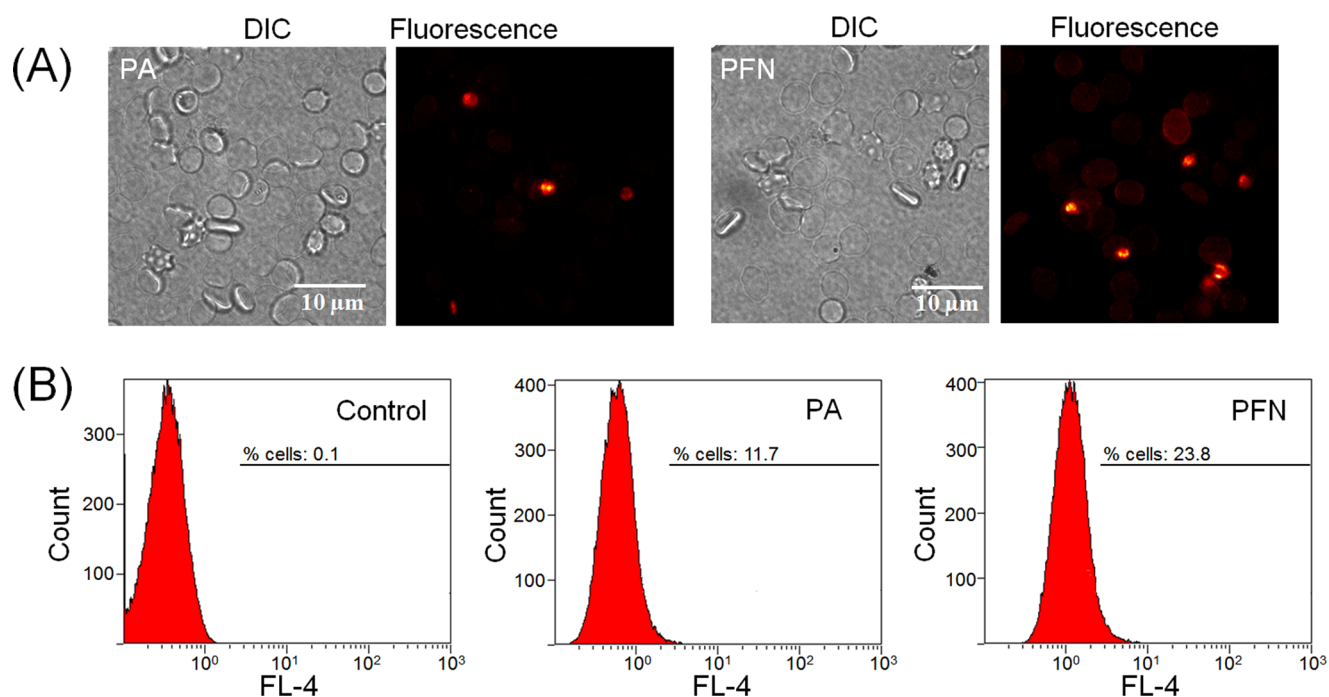


Figure 6. Fluorescence images of PA and PFNs in Plasmodium-infected erythrocytes. (A) Plasmodium-infected erythrocytes were incubated with PA ($0.16 \mu\text{M}$) or PFNs ($25 \mu\text{g/mL}$) in a culture medium for 1 h at 37°C . The uptake efficiencies of PA and PFNs were quantified by flow cytometric analysis (B).

249 As shown in Figure 7B, there was a difference in the reduction
250 of infection rates between PAs ($0.32 \mu\text{M}$) and PFNs ($50 \mu\text{g}/$
251 mL) after irradiation with LED light. The concentration of PA

($0.32 \mu\text{M}$) was equivalent to the concentration of PA molecules
252 bonded to the surfaces of the PFNs ($50 \mu\text{g/mL}$). PFNs resulted
253 in a greater reduction in infection during the initial 15 min and
254

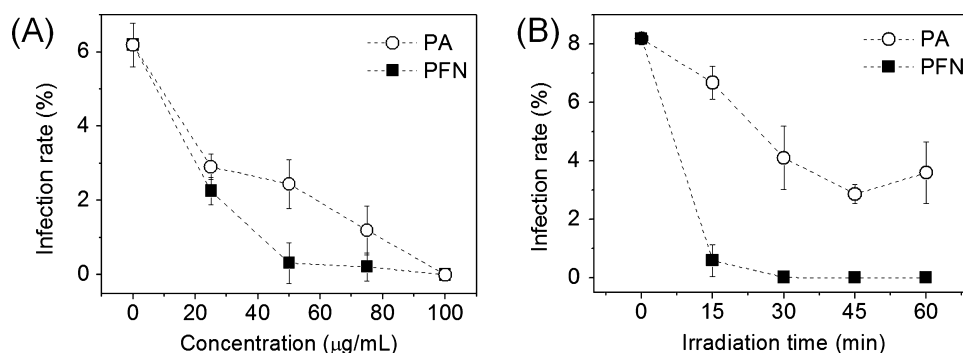


Figure 7. PDI of *P. falciparum* according to (A) the concentration of PDI agents (PAs and PFNs) and (B) LED irradiation time. The experiments were repeated in triplicate.

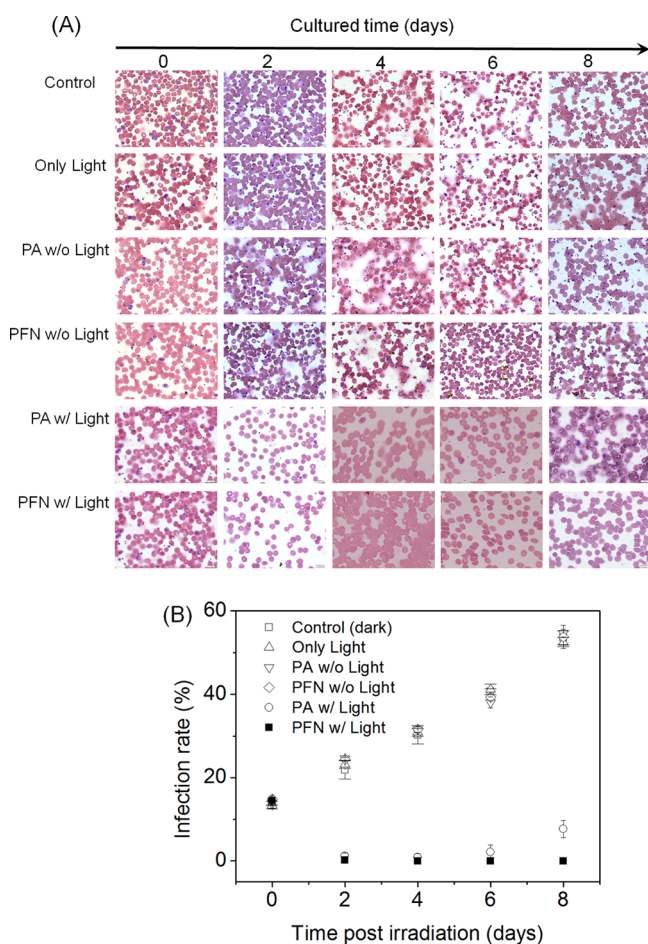


Figure 8. *P. falciparum* eradication at 8 days after PDI treatment. Plasmodium-infected erythrocytes were visualized by Giemsa staining. Magnified stained images of control (dark), only light, PA/PFN without light, and PA-/PFN-mediated PDI treatments are shown in (A). (B) Infection rates were quantified as a function of time. The experiments were repeated in triplicate.

Table 1. Change of the C_t Values of the *P. falciparum* CSP Gene and pLDH Gene by RT-PCR^a

gene	treatment	0 days	2 days	4 days	6 days	8 days
<i>P.f.</i> ^b CSP ^c gene	control	27.33	29.61	29.62	28.42	24.88
	PA	27.13	33.39	33.8	31.67	29.41
	PFNs	28.5	N/A	N/A	N/A	N/A
<i>P.f.</i> pLDH ^d gene	control	27.51	30.12	30.24	28.87	25.06
	PA	27.67	34.04	34.35	32.39	30.09
	PFNs	27.52	N/A	N/A	N/A	N/A

^aControl, PAs, and PFNs represent the light-only condition without PDI agents and the conditions of PDI treatments with PA and PFNs, respectively. ^b*P. falciparum*. ^cCircumsporozoite protein. ^dPlasmodium lactate dehydrogenase.

also incubated with PDI treatment for only 30 min of the initial 264 period with PAs (0.48 µM) or PFNs (75 µg/mL). Every 2 days, 265 the proliferation of the malarial parasites was assessed by 266 Giemsa staining and the RT-PCR assay. As shown in Figure 8B, 267 the infection rates of *P. falciparum* were continuously increased 268 in the cases of the light-only condition without the PDI agents 269 and the PDI agents-only condition without irradiation. In the 270 case of PDI treatment with PA, the infection rate increased 271 again after 4 days and the malarial parasite count increased 272 again after 6 days. In contrast, the infection rate did not 273 increase after PDI treatment using PFNs and erythrocyte 274 rupture did not occur (see Figure 8A). In addition, the RT- 275 PCR analysis indicates that the lower the C_t value, the more the 276 number of genes present, as shown in Table 1. 277

CONCLUSIONS

We fabricated MNPs coupled to PA molecules using a simple 279 modification process. The fabricated PFNs were characterized 280 by SEM, XRD, FT-IR, absorption spectroscopy, and emission 281 spectroscopy. The PFNs generated singlet oxygens, as 282 confirmed by time-resolved near-IR spectroscopy. A compar- 283 ison of PDI treatment with PAs and PFNs showed that 284 Plasmodium-infected erythrocytes were more effectively treated 285 with PFN/PDI than with PA/PDI due to the EPR effect of 286 PFNs. More importantly, PDI treatment with PFNs eradicated 287 the malarial parasite from the erythrocytes without recurrence 288 after 8 days. 289

AUTHOR INFORMATION

Corresponding Authors

*E-mail: malarim@korea.ac.kr. Tel: +82-2626-3245. Fax: +82- 292 2-2626-1465 (C.S.L.). 293

255 a 0% infection rate after 30 min. In contrast, PA molecules 256 reduced the infection rate to only 56% of that of PFNs over the 257 same time period. This suggests that PFNs are more effective 258 than PAs for PDI treatment of Plasmodium-infected eryth- 259 rocytes.

260 The Plasmodium-infected erythrocytes were incubated for 8 261 more days after only light irradiation for 30 min without PDI 262 agents (PAs or PFNs) and incubated for 8 days with only PA 263 (0.48 µM) or PFNs (75 µg/mL) without light irradiation, and

294 *E-mail: yrkim@yonsei.ac.kr. Tel: +82- 2123-2646. Fax: +82-2-
295 364-7050 (Y.-R.K.).

296 ORCID 

297 Yong-Rok Kim: 0000-0001-8166-9889

298 Author Contributions

299 ^{||}K.-K.W., J.W.J., E.P.S., and H.Y.S. contributed equally to this
300 manuscript.

301 Author Contributions

302 All authors contributed to the writing of this manuscript and
303 have approved the final version of the manuscript.

304 Notes

305 The authors declare no competing financial interest.

306 ACKNOWLEDGMENTS

307 This work was carried out with the support of the “Cooperative
308 Research Program for Agriculture Science & Technology
309 Development (Project No. PJ01083001)” Rural Development
310 Administration, Republic of Korea, and by a grant from the
311 National Research Foundation (NRF) of Korea, funded by the
312 Korea government (MSIP) (No. NRF-2016R1A2B4011155).

313 REFERENCES

- 314 (1) LeBlanc, D.; Story, R.; Gross, E. Laser-Induced Inactivation of
315 *Plasmodium falciparum*. *Malar. J.* **2012**, *11*, 267.
- 316 (2) Maier, A. G.; Cooke, B. M.; Cowman, A. F.; Tilley, L. Malaria
317 Parasite Proteins That Remodel the Host Erythrocyte. *Nat. Rev.*
318 *Microbiol.* **2009**, *7*, 341–354.
- 319 (3) Augustine, A. D.; Hall, B. F.; Leitner, W. W.; Mo, A. X.; Wali, T.
320 M.; Fauci, A. S. Niaid Workshop on Immunity to Malaria: Addressing
321 Immunological Challenges. *Nat. Immunol.* **2009**, *10*, 673–678.
- 322 (4) Sidhu, A. B. S.; Verdier-Pinard, D.; Fidock, D. A. Chloroquine
323 Resistance in *Plasmodium falciparum* Malaria Parasites Conferred by
324 pfprt Mutations. *Science* **2002**, *298*, 210–213.
- 325 (5) Chango, A.; Abdennebi-Najar, L. Folate Metabolism Pathway and
326 *Plasmodium falciparum* Malaria Infection in Pregnancy. *Nutr. Rev.*
327 **2011**, *69*, 34–40.
- 328 (6) Ridley, R. G. Medical Need, Scientific Opportunity and the Drive
329 for Antimalarial Drugs. *Nature* **2002**, *415*, 686–693.
- 330 (7) Le Bras, J.; Durand, R. The Mechanisms of Resistance to
331 Antimalarial Drugs in *Plasmodium falciparum*. *Fundam. Clin.*
332 *Pharmacol.* **2003**, *17*, 147–153.
- 333 (8) Zhao, X.-J.; Lustigman, S.; Kenney, M. E.; Ben-Hur, E. Structure-
334 Activity and Mechanism Studies on Silicon Phthalocyanines with
335 *Plasmodium falciparum* in the Dark and under Red Light. *Photochem.*
336 *Photobiol.* **1997**, *66*, 282–287.
- 337 (9) Kashef, N.; Abadi, G. R. S.; Djavid, G. E. Phototoxicity of
338 Phenothiazinium Dyes against Methicillin-Resistant *Staphylococcus*
339 *aureus* and Multi-Drug Resistant *Escherichia coli*. *Photodiagn. Photodyn.*
340 *Ther.* **2012**, *9*, 11–15.
- 341 (10) Huang, P.; Li, Z. M.; Lin, J.; Yang, D. P.; Gao, G.; Xu, C.; Bao,
342 L.; Zhang, C. L.; Wang, K.; Song, H.; Hu, H. Y.; Cui, D. X.
343 Photosensitizer-Conjugated Magnetic Nanoparticles for in Vivo
344 Simultaneous Magnetofluorescent Imaging and Targeting Therapy.
345 *Biomaterials* **2011**, *32*, 3447–3458.
- 346 (11) Hajri, A.; Wack, S.; Meyer, C.; Smith, M. K.; Leberquier, C.;
347 Keding, M.; Aprahamian, M. In Vitro and in Vivo Efficacy of
348 Photofrin (R) and Pheophorbide A, a Bacteriochlorin, in Photo-
349 dynamic Therapy of Colonic Cancer Cells. *Photochem. Photobiol.* **2002**,
350 *75*, 140–148.
- 351 (12) Baptista, M. S.; Wainwright, M. Photodynamic Antimicrobial
352 Chemotherapy (Pact) for the Treatment of Malaria, Leishmaniasis and
353 Trypanosomiasis. *Braz. J. Med. Biol. Res.* **2011**, *44*, 1–10.
- 354 (13) Zhou, Z.; Song, J.; Nie, L.; Chen, X. Reactive Oxygen Species
355 Generating Systems Meeting Challenges of Photodynamic Cancer
356 Therapy. *Chem. Soc. Rev.* **2016**, *45*, 6597–6626.

- (14) Shi, S.; Liu, Y.; Chen, Y.; Zhang, Z.; Ding, Y.; Wu, Z.; Yin, J.;
Nie, L. Versatile Ph-Response Micelles with High Cell-Penetrating
358 Helical Diblock Copolymers for Photoacoustic Imaging Guided
359 Synergistic Chemo-Photothermal Therapy. *Theranostics* **2016**, *6*,
2170–2182. 361
- (15) Liu, Y.; Kang, N.; Lv, J.; Zhou, Z. J.; Zhao, Q. L.; Ma, L. C.;
362 Chen, Z.; Ren, L.; Nie, L. M. Deep Photoacoustic/Luminescence/
363 Magnetic Resonance Multimodal Imaging in Living Subjects Using
364 High-Efficiency Upconversion Nanocomposites. *Adv. Mater.* **2016**, *28*,
6411–6419. 366
- (16) Yin, T.; Huang, P.; Gao, G.; Shapter, J. G.; Shen, Y.; Sun, R.;
367 Yue, C.; Zhang, C.; Liu, Y.; Zhou, S.; Cui, D. Superparamagnetic
368 Fe₃O₄-Peg2k-Fa@Ce6 Nanoprobes for in Vivo Dual-Mode Imaging
369 and Targeted Photodynamic Therapy. *Sci. Rep.* **2016**, *6*, No. 36187. 370
- (17) Choi, K. H.; Lee, H. J.; Park, B. J.; Wang, K. K.; Shin, E. P.; Park,
371 J. C.; Kim, Y. K.; Oh, M. K.; Kim, Y. R. Photosensitizer and
372 Vancomycin-Conjugated Novel Multifunctional Magnetic Particles as
373 Photoinactivation Agents for Selective Killing of Pathogenic Bacteria.
374 *Chem. Commun.* **2012**, *48*, 4591–4593. 375
- (18) Deng, H.; Li, X. L.; Peng, Q.; Wang, X.; Chen, J. P.; Li, Y. D.
376 Monodisperse Magnetic Single-Crystal Ferrite Microspheres. *Angew.*
377 *Chem., Int. Ed.* **2005**, *44*, 2782–2785. 378
- (19) Huang, Y. N.; Zhang, L. P.; Huan, W. W.; Liang, X. J.; Liu, X.
379 N.; Yang, Y. X. A Study on Synthesis and Properties of Fe₃O₄
380 Nanoparticles by Solvothermal Method. *Glass Phys. Chem.* **2010**, *36*,
325–331. 382
- (20) Choi, K. H.; Wang, K. K.; Shin, E. P.; Oh, S. L.; Jung, J. S.; Kim,
383 H. K.; Kim, Y. R. Water-Soluble Magnetic Nanoparticles Function-
384 alized with Photosensitizer for Photocatalytic Application. *J. Phys.*
385 *Chem. C* **2011**, *115*, 3212–3219. 386
- (21) Wang, K. K.; Jung, M. S.; Choi, K. H.; Shin, H. W.; Oh, S. I.; Im,
387 J. E.; Kim, D. H.; Kim, Y. R. Fabrication and Photophysical Properties
388 of Singlet Oxygen Generating Nanoporous Membrane. *Surf. Coat.*
389 *Technol.* **2011**, *205*, 3905–3908. 390
- (22) Stanic, D. I.; Liu, X. Q.; De, S. L.; Batzloff, M. R.; Forbes, T.;
391 Davis, C. B.; Sekuloski, S.; Chavchich, M.; Chung, W.; Trenholme, K.;
392 McCarthy, J. S.; Li, T.; Sim, B. K. L.; Hoffman, S. L.; Good, M. F.
393 Development of Cultured *Plasmodium falciparum* Blood-Stage Malaria
394 Cell Banks for Early Phase in Vivo Clinical Trial Assessment of Anti-
395 Malaria Drugs and Vaccines. *Malar. J.* **2015**, *14*, 143–150. 396
- (23) Sathpathi, S.; Mohanty, A. K.; Satpathi, P.; Mishra, S. K.; Behera,
397 P. K.; Patel, G.; Dondorp, A. M. Comparing Leishman and Giemsa
398 Staining for the Assessment of Peripheral Blood Smear Preparations in
399 a Malaria-Endemic Region in India. *Malar. J.* **2014**, *13*, 512. 400
- (24) Drmota, A.; Kosak, A.; Znidarsic, A. A Mechanism for the
401 Adsorption of Carboxylic Acids onto the Surface of Magnetic
402 Nanoparticles. *Mater. Technol.* **2008**, *42*, 79–83. 403
- (25) Wu, N. Q.; Fu, L.; Su, M.; Aslam, M.; Wong, K. C.; Dravid, V. P.
404 Interaction of Fatty Acid Monolayers with Cobalt Nanoparticles. *Nano*
405 *Let.* **2004**, *4*, 383–386. 406
- (26) Jacintho, G. V. M.; Brolo, A. G.; Corio, P.; Suarez, P. A. Z.;
407 Rubim, J. C. Structural Investigation of Mfe₂O₄ (M = Fe, Co)
408 Magnetic Fluids. *J. Phys. Chem. C* **2009**, *113*, 7684–7691. 409
- (27) Nafujjaman, M.; Revuri, V.; Nurunnabi, M.; Cho, K. J.; Lee, Y.
410 K. Photosensitizer Conjugated Iron Oxide Nanoparticles for
411 Simultaneous in Vitro Magneto-Fluorescent Imaging Guided Photo-
412 dynamic Therapy. *Chem. Commun.* **2015**, *51*, 5687–5690. 413
- (28) Wang, K.-K.; Li, J.; Kim, B.-J.; Lee, J.-H.; Shin, H.-W.; Ko, S.-H.;
414 Lee, W.-Y.; Lee, C.-H.; Jung, S. H.; Kim, Y.-R. Photophysical
415 Properties of Pheophorbide-a Derivatives and Their Photodynamic
416 Therapeutic Effects on a Tumor Cell Line in Vitro. *Int. J. Photoenergy*
417 **2014**, *2014*, 1–7. 418
- (29) Paonessa, R. S.; Trogler, W. C. Solvent-Dependent Reactions of
419 Carbon-Dioxide with a Platinum(II) Dihydride - Reversible Formation
420 of a Platinum(II) Formatehydride and a Cationic Platinum(II) Dimer,
421 [Pt₂H₃(PEt₃)₄][HCO₂]. *J. Am. Chem. Soc.* **1982**, *104*, 3529–3530. 422
- (30) Prabhakar, U.; Maeda, H.; Jain, R. K.; Sevik-Muraca, E. M.;
423 Zamboni, W.; Farokhzad, O. C.; Barry, S. T.; Gabizon, A.; Grodzinski,
424 P.; Blakey, D. C. Challenges and Key Considerations of the Enhanced
425

- 426 Permeability and Retention Effect for Nanomedicine Drug Delivery in
427 Oncology. *Cancer Res.* **2013**, *73*, 2412–2417.
- 428 (31) Shi, H.; Liu, Z.; Li, A.; Yin, J.; Chong, A. G.; Tan, K. S.; Zhang,
429 Y.; Lim, C. T. Life Cycle-Dependent Cytoskeletal Modifications in
430 *Plasmodium falciparum* Infected Erythrocytes. *PLoS One* **2013**, *8*,
431 No. e61170.
- 432 (32) Santos-Magalhães, N. S.; Mosqueira, V. C. Nanotechnology
433 Applied to the Treatment of Malaria. *Adv. Drug Delivery Rev.* **2010**, *62*,
434 560–575.